Characterisation of Waveguide Microcavities using High-Resolution Transmission Spectroscopy and Near-field Scanning Optical Microscopy

G. H. Vander Rhodes, M. S. Ünlü, B. B. Goldberg
Departments of Physics and Electrical and Computer Engineering and the Photonics Center, Boston University, 8 Saint Mary's St., Boston, MA 02215-2421 USA

J. M. Pomeroy
Department of Physics, Cornell University, Ithaca, NY 14853-2501, USA

T. F. Krauss
Optoelectronics Group, Department of Electronics and Electrical Engineering, Glasgow University, Glasgow G12 8LT, Scotland, United Kingdom

Abstract

A wide variety of optoelectronic devices with novel gratings are being created for which knowledge of the internal optical fields and details of loss mechanisms are highly desirable. To this end, we have built apparatus and developed techniques for simultaneous measurement of the scattered and evanescent fields in the near field of the active region of grating-type waveguide devices combined with high-resolution transmission measurements. Here we report characterisation and analysis of a waveguide microcavity. Our transmission scans improve greatly on previous measurements, showing detailed structure which we explain using transfer matrix simulations including the structure of the input and output waveguides of the device. We also present near-field scanning optical microscopy data of the active region of the waveguide. Internal mode patterns and height dependent data, when compared with simulations of the electric field magnitude, show that the device may suffer from significant scattering at the grating interfaces.

Keywords
Near-field Scanning Optical Microscopy, Photonic Microcavity, Photonic Bandgap plates

I. INTRODUCTION

There are many problems that need to be solved in order to advance the usage, design, and applicability of the many new photonic crystal-based devices.[1] New fabrication techniques need to be developed, including investigations into different material systems and unique methods of making large two and three-dimensional structures with superior large-scale periodicity. Also important is the evolution of simulation methods which are well suited to these structures. The additional development of new techniques of device characterisation are critical to relate simulated device parameters to direct measurement of internal optical modes. We have built a dedicated instrument capable of performing simultaneous high-resolution transmission spectroscopy and near-field scanning optical microscopy (NSOM).[2],[3] We demonstrate the value of our direct diagnostic characterisation technique with a detailed study of a waveguide microcavity photonic bandgap device.

II. EXPERIMENTAL SETUP

A schematic diagram of our instrument is shown in figure 1. For excitation, a tunable CW Ti:Sapphire laser (output ≈10 mW) was launched into a lensed fibre and coupled into the input of the waveguide. The exit facet of the waveguide was imaged with an objective and the transmitted light was split to an infrared video camera for visual inspection and to a cooled Ge detector [4] for transmission measurements. Since the sample needed to remain stationary, a tip-scanning near-field scanning optical microscope was positioned above the waveguide region of study. The NSOM probe, a tapered single mode optical fibre,[3] was held in close proximity to the surface with shear-force feedback.[5],[6] This provided simultaneous topography with collection mode optical imaging. The optical signal collected with the NSOM probe included evanescent fields coupled out from the surface by the presence of the dielectric tip medium, allowing the electric field magnitudes around the active grating region of the optoelectronic devices to be directly measured.[7]

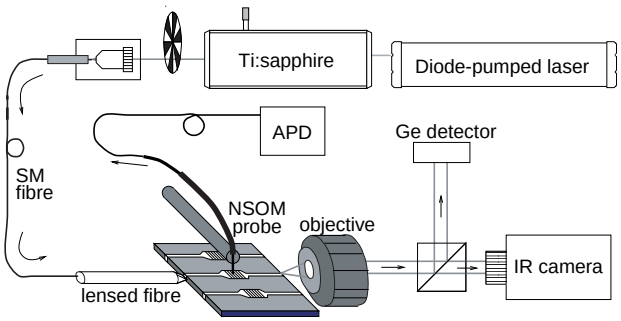

Figure 1: Experimental setup schematic showing the tunable Ti:Sapphire used for excitation, optical chopper, single-mode fibre launch, and lensed fibre used to launch light into the waveguide device.The NSOM probe was positioned above the waveguide region of interest, and the exit facet was imaged with an objective and the transmitted light was split to an infrared video camera for visual inspection and to a cooled Ge detector for transmission measurements

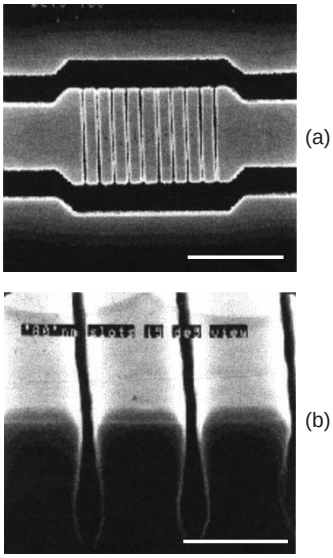

Figure 2: Scanning electron microscope (SEM) photographs of the device under test. The top image (a) shows an overview of a device with 10 air gaps; the scale bar indicates a size of 3 μm.Though indistinct in the micrograph, the spacing between the two central air gaps is 60 nm wider than the periodic spacing of 480 nm between all other air gaps. The bottom image (b) shows a closeup of two of these air gaps, clearly showing the shape of the sidewalls; the scale bar is 400 nm.

III. DEVICE UNDER TEST

The device under test, shown in figure 2, is a waveguide based Bragg grating with a small number of periods, designed to have a third order transmission stop band in the near infrared. A defect in the Bragg layers gives rise to a high-Q resonance in the centre of the stop band. The device was fabricated using an $Al_xGa_{1-x}As$ material system ($x = 0.12$ for guiding region, $x = 0.35$ for cladding), with etched trenches laterally defining the waveguide and semiconductor fin active region. The fins are separated by etched air gaps of 70 nm, with a centre fin that is 60 nm wider than the other fins, resulting in the aforementioned resonance in transmission. The design improves on earlier devices [8] with deeper etched slots and a modified transition between the input waveguide and active regions of the device. Due to the high index contrast between the Bragg layers, very high reflectivities and high Q resonances can be achieved in a few period device, and could be easily incorporated into AlGaAs optoelectronic device systems. Two samples were used, one with a 400 nm periodicity (sample A), and the other with a 460 nm periodicity (sample B).

IV. TRANSMISSION

Detailed transmission experiments were carried out to fully characterise the wavelength dependence of the device, which was then compared to simulations. Figure 3a shows the transmission versus wavelength for the long-wavelength band edge of sample A. The spectrum was normalised to the transmission through an adjacent waveguide without a Bragg grating region, smoothed to remove extraneous cavity effects of the reference waveguide. A high density of points in wavelength were taken to resolve the additional beating in the device. These high frequency oscillations were caused by the additional cavity effects due to the slightly mismatched lengths of the input and output waveguides to the Bragg region. A transfer matrix method [9] simulation that combines these details with an 18 nm “oxide skin” [8] and indices of refraction taken from an effective index model [9] gave the spectrum in figure 3b, which reproduces well the frequency dependence of the measured data. Note, however, the low overall transmission, a point addressed in detail below.

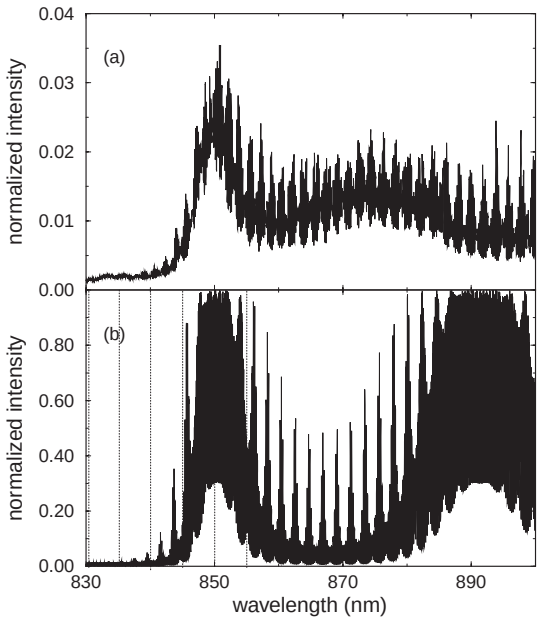

Figure 3: Transmission spectroscopy at the long-wavelength band-edge in sample A. Figure (a) is a measured transmission spectrum that shows very well the band-edge, as well as the first and second band-edge resonances. The high frequency oscillations were caused by the additional cavity effects due to the slightly mismatched lengths of the input and output waveguides. A simulated effective index TMM simulation in (b) shows that our data reproduces the positions of the band-edge and band-edge resonance predicted by the model, as well as the additional beating. Also note the significantly decreased overall transmission.

Figure 4a shows transmission spectra for the wavelength region that includes the short-wavelength band edge and defect of sample B. We see again low overall transmission, as well as two relatively low-Q defect resonances. Because we were using a fibre-launched system, we did not have good control of polarisation, and have included both TE and TM modes in the model calculations shown in figure 4b. The data reproduce the two defect resonances, as well as the short wavelength band edge.

Unlike previous work on similar devices, [8] our high-resolution normalised spectral transmission scans show the importance of including the appropriate input and output mode coupling in simulations. Yet the overall transmission is significantly lower than predicted and the measured resonances have a much reduced Q, even when compared to previ-

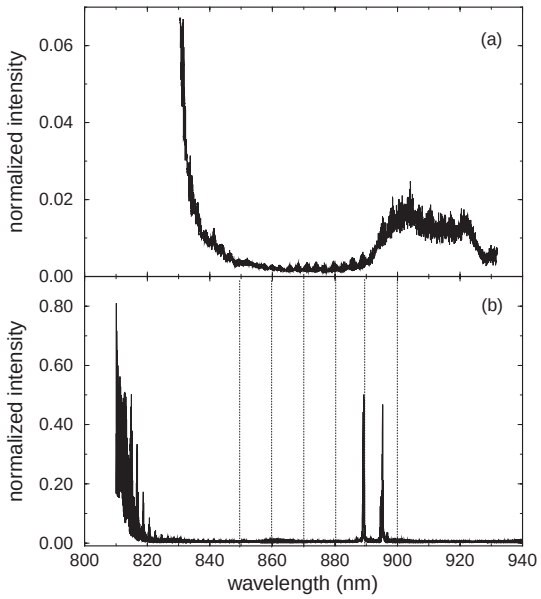

Figure 4: Transmission spectroscopy around the defect wavelengths in sample B. The measured transmission spectrum is in figure (a), which shows the short-wavelength band-edge as well as two very broad defect resonances. The existence of two resonances indicates that both TE and TM modes are excited in the waveguide device. We included this in the simulation (b) by adding a TE mode model to a TM mode model and renormalising.

ous measurements. Full three-dimensional simulations [11] predict that this device supports many different modes -- we believe that the discrepancy between previous work and our measurements may be due to a difference in mode coupling. In addition, loss in the system would not only naturally reduce overall transmission, but also lower the Q factor, due to an effective drop in the number of passes in the cavity. [10] In an effort to include this in our simulations we have introduced absorption-related imaginary terms to the indices of refraction and observed a correlation between increased absorption and lower-Q resonances, but quantitative conclusions based upon the simulations are premature at the present stage.

V. NSOM MEASUREMENTS

Defect-localised photon states are used in many optoelectronic devices, including photodetectors, [12] semiconductor lasers, [13],[14] and nanometer-scale light guiding structures.[15] The ability to map out regions of increased optical density, as well as other spatial optical modes would be a useful characterisation tool providing critical feedback to photonic bandgap-based device designers. Understanding the mode structure is a very valuable diagnostic tool, particularly for devices, which for one reason or another, do not correlate well with simulations. However, since these modes are largely internal with weak evanescent surface fields, they cannot be probed by conventional far-field techniques. [16] A proximity probe such as NSOM can measure these local internal modes by providing a weak, non-perturbative coupling mode for the surface evanescent field components. [7]

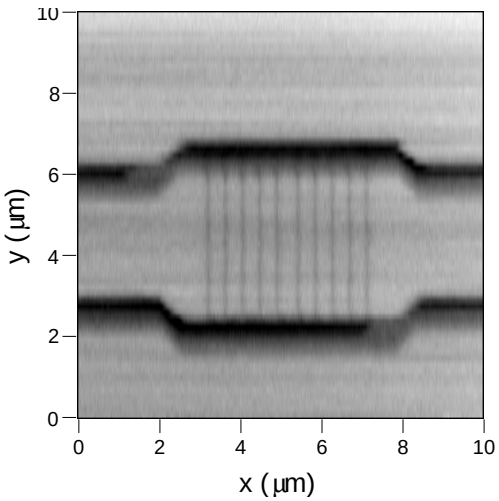

Figure 5: Representative topographic image, demonstrating good spatial resolution that agrees favourably with the SEM micrographs in figure 2. The area imaged in figures 6 and 7 is smaller, only the middle 5 μ m square.

A representative topographic image, taken simultaneously with the optical mode scans, is displayed in figure 5. The image demonstrates good spatial resolution that agrees with SEM micrographs. This level of resolution in the force microscopy images allows us to make quantitative measurements of device dimensions, as well as anchoring the spatial mode scans to physical device structures. The area imaged in successive scans is smaller: only the middle 5 μ m x 5 μ m.

The band edge spatial modes we show in figure 6 are for a device with similar transmission characteristics to figure 3. We compare three scans: one taken well within the stop band, one at the mid-point of the band edge, and one at the top of the

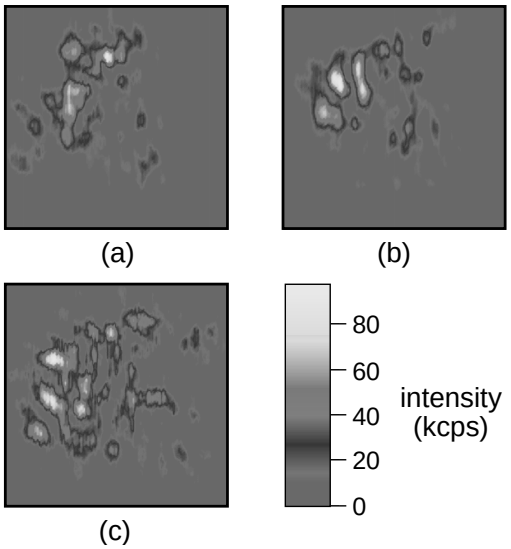

Figure 6: Band-edge spatial modes, with light entering the images from the left. Here, three wavelengths are compared: (a) well within the stop band, (b) at the mid-point of the band-edge, and (c) at the top of the first band-edge resonance. The colour bar shows the intensity of the signal measured, in units of kilo counts per second. These mode patterns show greater penetration of the field as the frequency is tuned from the stop-band into the pass-band, as one might expect.

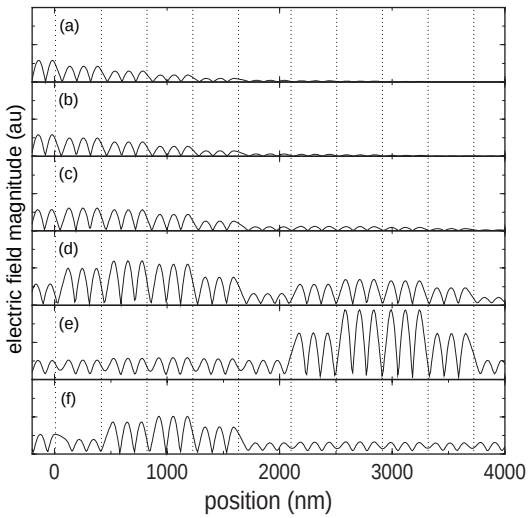

Figure 7: Electric field magnitude simulations performed using an S-matrix method at the wavelengths indicated in figure 3. Because these wavelengths are within the stop-band, (a) -- (c) show well the exponential damping of the field, while (d) -- (f) exhibit constructive interference behaviour that results in a large field magnitude at the end of the structure. Also shown in this figure are the positions of the centres of the air gaps, indicated by dotted lines.

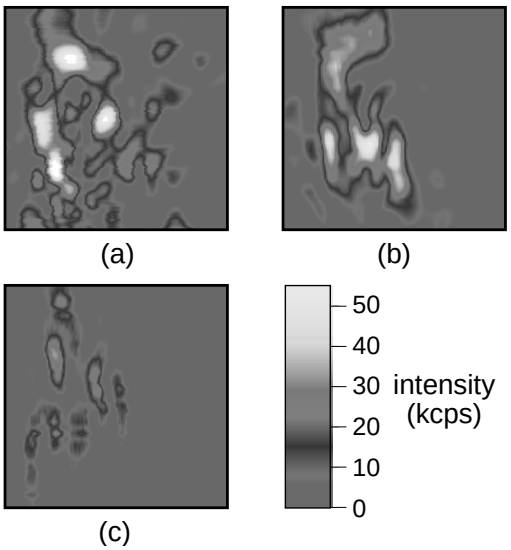

Figure 8: Spatial modes taken around the defect wavelengths. Compared in this figure are spatial modes taken (a) shorter than the defect wavelength, (b) at the defect wavelength, and (c) longer than the defect wavelength. The defect scan shows bright spots towards the middle of the device, while the other wavelengths show bright spots towards the input end, with exponential damping in the direction of propagation.

first band edge resonance. Note that these mode patterns show greater penetration of the field as the frequency is tuned from the stop-band into the pass-band, as one might expect. For comparison, figure 7 shows S-matrix [17] simulations of electric field magnitude at the 6 wavelengths indicated in figure 3b. The simulations show exponential damping along the direction of propagation, as expected, for wavelengths within the stop band. As the band edge is approached, constructive interference behaviour arises that results in a large electric field magnitude at the end of the structure.

We performed similar experiments and further analysis in the defect region of the transmission curve. Figure 8 compares a scan at the defect wavelength to shorter and longer wavelengths on either side of the defect resonance frequency. The defect scan (figure 8b) shows bright spots towards the middle of the device, while the other wavelengths show bright spots towards the input end, with exponential damping in the direction of propagation. Figure 9 shows electric field magnitude simulations for this wavelength region, comparing the wavelengths indicated in figure 4. Again, as expected, the band gap scans exhibit exponential damping, and the defect wavelength shows strong localisation of light at the defect fin.

VI. SCATTERING

We see many of the same themes in both the simulations and measurements: exponential damping in the stop band and localisation at the defect wavelength. However, there is clear quantitative disagreement. To fully understand devices such as these, more sophisticated two- and three-dimensional simulations need to be used; also we must understand the origin of the light that we are coupling into our tip.

To gain this understanding, we first note that in general, evanescent fields have an exponential dependence on z, the distance between the tip and sample, with a well-defined decay constant, while scattered radiation will not. We performed scans in the x-z plane to examine this dependence, where x is along the waveguide (figure 10). Line cuts of this image in the vertical direction show no exponential dependence with decay constants close to expected values, where the *1/e* point is approximately 50 nm. The intensity oscillations in the z direction throughout the image have a periodicity that

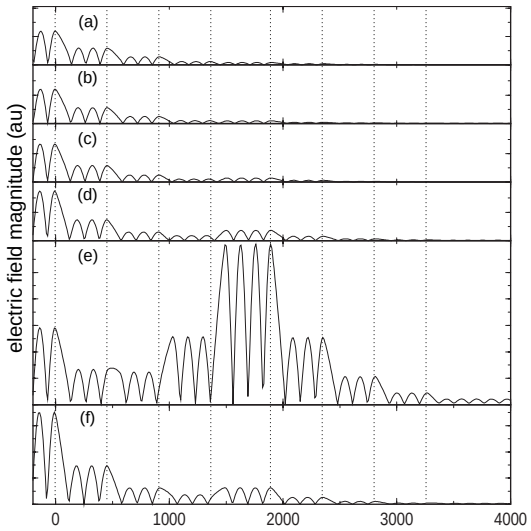

Figure 9: Electric field magnitude simulations performed at the wavelengths indicated in figure 4. As expected, the band gap simulations (all but (e)) exhibit exponential damping, and the defect wavelength simulation (e) shows strong localisation of light at the defect fin.

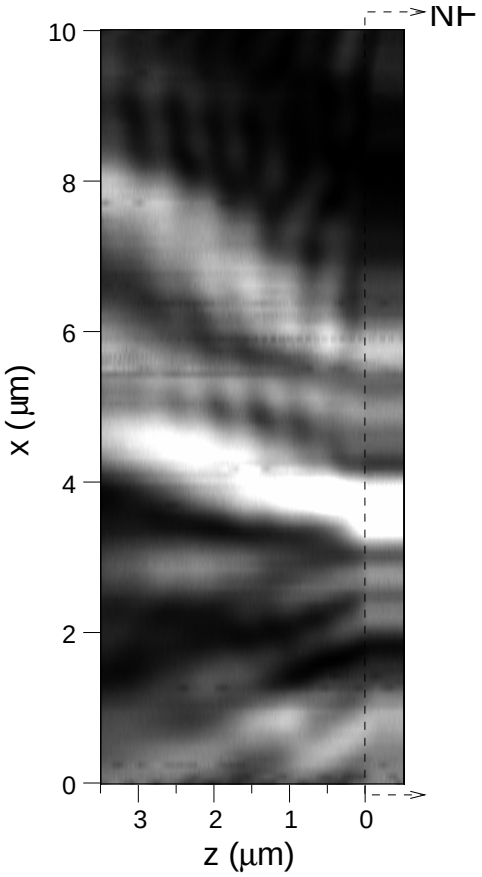

Figure 10: A gray scale image showing the intensity of collected radiation varying both the height about the device (z) and along the waveguide (x). The waveguide of sample A was excited at 860 nm at the long wavelength band-edge resonance. Note the lack of exponential decay expected of evanescent modes, as well as the overall diffraction pattern typical of multiply in-phase scattering centres.

indicates that they are caused by interference between the tip and the sample. In addition, we also observe what appears to be a diffraction pattern in the angled and interfering propagation. Since the device is being excited by a coherent source, scattered radiation could lead to such a pattern. [10] The lack of evidence of exponential decay and the significant intensity detected many μm away from the surface leads us to believe that most of the optical signal we collect is due to scattered light, preventing us from imaging the evanescent fields.

This large amount of scattering is consistent with the low overall transmission and low-Q resonances of the defect. One reason for this level of scattering would be a rough top surface, scattering the waveguide modes into free-space propagating modes. However, AFM measurements show that the highest RMS roughness observed in a power spectrum was only a few nm. However, side wall roughness in the air gap region could still account for our observations. This Raleigh scattering in Bragg grating devices has also been observed, [18] and may be indicative of the mode structure overlap with enhanced scattering regions. We also investigated the etched trenches defining the waveguide as another possible sources of scatter. We performed x-z scans away from the Bragg grating region, and observed 2 orders of magnitude reduction in collected light, which was still enough to overwhelm the predicted strong coupling of evanescent fields. This might point to the roughness of these etched trenches also contributing to scattering loss.

VII. SUMMARY

In summary, with high-resolution transmission spectroscopy, we were able to identify limitations in the performance of a photonic-crystal based device. Through comparison with simulations of the electric field magnitude, we used NSOM to determine possible reasons for these limitations. Through height dependent scans, we showed that there is a significant amount of scattering, possibly due to roughness of the sidewalls in the air gap regions and waveguide-defining trench regions. This scattering loss can explain the discrepancies between the measured transmission spectra and a transfer matrix model.

Our future efforts will be focusing first on increasing our signal to noise ratio in order to observe the exponential damping of the evanescent field that we expect, next on using other methods to verify our NSOM scattering measurements, including far-field observation. Lastly, we will be applying these techniques to new types of photonic-bandgap microcavities [19] that benefit from the use of sophisticated multidimensional simulations at both the design stage as well as the diagnostic stage. With these new devices, we hope to show that NSOM can not only be used as a diagnostic technique, but also truly as a way of measuring internal spatial modes.

VIII. REFERENCES

[1] YABLONOVITCH, E., 'Photonic band-gap structures,' *J. Opt. Soc. Am. B*, 1993, **10** (2), pp. 283-295

[2] DURIG, U., POHL, D. W., and ROHNER, F., 'Near-field optical scanning microscopy,' *J. Appl. Phys.*, 1986, **59** p. 3318

[3] BETZIG, E., TRAUTMAN, J. K., HARRIS, T. D., WEINER, J. S., and KOSTELAK, R. L., 'Breaking the diffraction barrier: Optical microscopy on a nanometric scale,' *Science*, 1991, **251** p. 1468

[4] Ge detector was obtained from EG&G, model # J16TE2-HSA2-R05M-HS

[5] BETZIG, E., FINN, P. L., and WEINER, J. S., 'Combined shear force and near-field scanning optical microscopy,' *Appl. Phys. Lett.*,1992, **60** p. 2484

[6] KARRAI, K. AND GROBER, R. D., 'Piezoelectric tip-sample distance control for near field optical microscopes,' *Appl. Phys. Lett.*, 1995, **66** (14) pp. 1842-1844

[7] CHOO, A. G., JACKSON, H. E., THIEL, U., BRABANDER, G. N. D., and BOYD., J. T., 'Near field measurements of optical channel waveguides and directional couplers,' *Appl. Phys. Lett.*, 1994, **65** (8) pp. 947--949

[8] KRAUSS, T. F., VÖGELE, B., STANLEY, C. R., and DE LA RUE, R. M., 'Waveguide microcavity based on photonic microstructures,' *IEEE Photonics Tech. Lett.*, 1997, **9** (2) pp. 176--178

[9] BORN, M. and WOLF, E., 'Principles of Optics,' (Macmillan, New York, 1964)

[10] SALEH, B. E. A. and TEICH, M. C., 'Fundamentals of Photonics,' (John Wiley and Sons, New York, 1991)

[11] VILLENEUVE, P. R., FAN, S., JOHNSON, S. G., and JOANNOPOULOS, J. D., 'Three-dimensional photon confinement in photonic crystals of low-dimensional periodicity,' *IEE Proceedings -- Optoelectronics, Special Issue on Photonic Crystals and Photonic Microstructures*, in press.

[12] ÜNLÜ, M. S. and STRITE, S., 'Resonant cavity enhanced photonic devices,' *J. Appl. Phys.*, 1995, **78** (2) pp. 607-639

[13] BULLOCK, D. L., SHIH, C. C., and MARGULIES, R. S., 'Photonic band structure investigation of two-dimensional Bragg reflector mirrors for semiconductor laser mode control,' *J. Opt. Soc. Am. B*, 1993, **10** (2) pp. 399-403

[14] KRAUSS, T. F., PAINTER, O., SCHERER, A., ROBERTS, J. S., and DE LA RUE, R. M., 'Photonic microstructures as laser mirrors,' *Optical Engineering*, 1998, **37** (4) pp. 1143-1148

[15] FAN, S., WINN, J. N., DEVENYI, A., CHEN, J. C., MEADE, R., and JOANNOPOULOS, J. D., 'Guided and defect modes in periodic dielectric waveguides,' *J. Opt. Soc. Am. B*, 1995, **12** (7) pp. 1267-1272

[16] TSAI, D. P., JACKSON, H. E., REDDICK, R. C, and WARMACK, S. H. S. R. J., 'Photon scanning tunneling microscopy study of optical waveguides,' *Appl. Phys. Lett.*, 1990, **56** (17) pp. 1515-1517

[17] YEH, P., 'Optical waves in layered media,' (Wiley, New York, 1988)

[18] CANNING, J., PSAILA, D. C., BRODZELI, Z., HIGLEY, A., and JANOS, M., 'Characterization of apodized fiber Bragg gatings for rejection filter applications,' *Applied Optics*, 1997, **36** , pp.9378-82

[19] FORESI, J. S., VILLENEUVE, P. R., FERRERA, J., THOEN, E. R., STEINMEYER, G., FAN, S., JOANNOPOULOS, J. D., KIMMERLING, L. C., SMITH, H. I., AND IPPEN, E. P., 'Photonic-bandgap microcavities in optical waveguides,' *Nature*, 1997, **390** (6656), pp. 143-145